Published in IET Microwaves, Antennas & Propagation
Received on 6th July 2010
Revised on 18th October 2010
doi: 10.1049/iet-map.2010.0281

ISSN 1751-8725

Full-wave semiconductor devices simulation using meshless and finite-difference time-domain approaches

R. Mirzavand[1] *A. Abdipour*[1] *G. Moradi*[1] *M. Movahhedi*[2]

[1]*Microwave/mm-wave & Wireless Communication Research Lab, Electrical Engineering Department, Radio Communications Center of Excellence, Amirkabir University of Technology, Tehran, Iran*
[2]*Electrical Engineering Department, Shahid Bahonar University of Kerman, Kerman, Iran*
E-mail: abdipour@aut.ac.ir

Abstract: A new numerical method for the full-wave physical modelling of semiconductor devices using a combination of the meshless and finite-difference time-domain (FDTD) approaches is described. The model consists of the electron equations for the active part and Maxwell's equations for the electromagnetic effects, which describe the complete behaviour of a high-frequency active device. The unconditionally stable method by using a semi-implicit meshless approach for the active model and the alternating-direction implicit (ADI)-FDTD approach for electromagnetic model leads to a significant decrease in the full-wave simulation time. Using this technique, we can achieve a 99% reduction in the computation time and obtain an acceptable degree of accuracy in comparison with conventional FDTD approaches. As the first step in the investigation, the authors use the electron flow equations without holes and recombination process as the semiconductor equations.

1 Introduction

The main issue in the global modelling of microwave circuits is the full-wave analysis of their active devices. In a full-wave analysis, the equations that describe the transport physics in conjunction with Maxwell's equations must be solved to predict the interactions between the carriers and the propagating wave inside the devices [1, 2]. Many different semiconductor simulating approaches have been developed in the past [2–5]. Fundamentally, all these techniques depend on the solution of the Poisson's equation along with the basic carrier transport equations. In this paper, the semiconductor analysis is based on the time-domain drift-diffusion method (DDM) [3]. The set of DDM equations contains Poisson's equation and the carrier transport equations, obtained by splitting the Boltzmann transport equation into its first two moments. The DDM model assumes that the carrier temperature is equal to the semiconductor lattice temperature. Therefore the carrier velocity is dependent on the electric field only. DDM is a simple technique with better convergence and shorter computational time in comparison with other more rigorous semiconductor numerical modelling. Thus, this simple modelling process is more suitable for use by a design engineer in the first step of the transistor's design, while in the next steps, one can use a more accurate model.

Recently, great effort has been devoted for developing meshless methods to find the numerical solution of partial differential equations [6]. The aim of these methods which are also called gridless, meshfree, element-free or cloud methods is to remove the connectivity information, that is, the mesh and only uses nodes to produce shape functions. In 1990, Kansa [7] introduced a new approach for this kind of problem, where the true solution is approximated for a linear combination of radial basis functions (RBF). This method has shown to be more efficient than traditional methods such as the, finite-difference methods and finite-element method [8, 9]. A major obstacle for the RBF collocation method is that the companion matrix is generally ill conditioned, non-symmetric and full dense, which constrains the applicability of the RBF method in solving large-scale problems. However, the compact RBF and the domain decomposition method can provide a way of reducing the computational time and the ill conditioning of the matrix [10, 11].

On the other hand, even for simple semiconductor equations, the simultaneous simulation of these equations and Maxwell's equations is time consuming because of limits on the simulation time-step size. In the last decade, a new method, called the alternating-direction implicit finite-difference time-domain (ADI-FDTD) method, has been introduced [12, 13] to solve Maxwell's curl equations. This method is an attractive alternative for the standard FDTD method because of its unconditional stability with moderate computational overhead. This means that the ADI-FDTD method is free of the Courant–Friedrich–Levy (CFL) stability restraint. ADI-FDTD can be useful for problems involving components with much smaller geometric features than the wavelengths of interest. The ADI approach has been used in the electromagnetic part of the semiconductor devices simulation [14, 15].

In the first part of this paper, we describe a semi-implicit meshless method for two-dimensional time-dependent simulation of semiconductor devices. In this method, the solution is approximated using the compact RBF. This allows solving problems with complex-shaped boundaries and forming fine or coarse points in locations where variable solutions change rapidly or slowly, respectively. On the other hand, the semi-implicit method allows the meshless method to be used for larger time steps without stability failures. The method is similar to implicit finite differences but can support arbitrary point locations. Because of the radial nature of the basis functions used, the schemes also make no distinction on the dimension of problem. In the second part, a combination of the meshfree and ADI-FDTD methods is used to solve the semiconductor electrical and electromagnetic equations. This allows using a larger time-step size that leads to significant CPU time reduction with acceptable accuracy.

2 Transistor physical model

The semiconductor models that are used are based on the moments of Boltzmann's transport equations obtained by integration over the momentum space. Three equations need to be solved along with Poisson's equation to obtain the quasi-static characteristics of the transistor. This system of coupled highly non-linear partial differential equations contains current continuity, energy conservation and momentum conservation equations [3]. The solution of this system of partial differential equations represents the complete hydrodynamic model. Simplified models are obtained neglecting some terms in the momentum equation. One of these simplified models is the drift-diffusion model (DDM) [16]. In this paper, we simulate a MESFET as a micro/mm-wave transistor that is a unipolar device. For this device, the equations to be solved in the DDM are [16]

$$\boldsymbol{J} = qn\mu_n(\boldsymbol{E}, N_{\mathrm{d}})\boldsymbol{E} + qD_n(\boldsymbol{E}, N_{\mathrm{d}})\nabla n \tag{1}$$

$$\frac{\partial n}{\partial t} = \frac{1}{q}\nabla \cdot \boldsymbol{J} \tag{2}$$

$$\nabla^2 \varphi = -\frac{q}{\varepsilon_0 \varepsilon_r}(N_{\mathrm{d}} - n) \tag{3}$$

where φ is the potential, $\boldsymbol{E} = -\nabla\varphi$, N_{d} is the doping profile, n is the electron (carrier) density, μ_n is the mobility coefficient and $D_n = \mu_n K_B T/q$. In this work, electron mobility has been considered as a function of doping and electric field [17]

$$\mu_n(E, N_{\mathrm{d}}) = \frac{\mu_0 + (v_{\mathrm{s}}/E)(E/E_{\mathrm{s}})^4}{1 + (E/E_{\mathrm{s}})^4} \tag{4}$$

while low-field mobility μ_0, saturation velocity v_{s} and critical field E_{s} (for the onset of negative differential mobility) are functions of doping N_{d}.

3 Meshless method based on RBF

The approximation of function $u^h(\boldsymbol{x})$, using RBF, may be written as a linear combination of N radial functions [18]

$$u^h(\boldsymbol{x}) = \sum_{i=1}^{N} \psi_i(\boldsymbol{x})a_i = \Psi^{\mathrm{T}}(\boldsymbol{x})\boldsymbol{a}; \quad \boldsymbol{x} \in R^d \tag{5}$$

where N is the number of data points, $\boldsymbol{x} = (x^1, x^2, \ldots, x^d)$ is the vector position, d is the dimension of the problem, $\psi_i(\boldsymbol{x}) = \psi(\boldsymbol{x}, \boldsymbol{x}_i)$ is a specific RBF of $\boldsymbol{x}$ and $\boldsymbol{x}_i$.

$\Psi(\boldsymbol{x}) = [\psi_1(\boldsymbol{x})\ \psi_2(\boldsymbol{x})\ \psi_N(\boldsymbol{x})]^{\mathrm{T}}$, and $\boldsymbol{a} = [a_1\ a_2\ \ldots\ a_N]^{\mathrm{T}}$ are coefficients to be determined. The matrix $\boldsymbol{a}$ can be determined by forcing the interpolation to pass through all N collocation points, resulting in

$$\begin{aligned}\boldsymbol{u} &= [u^h(\boldsymbol{x}_1), u^h(\boldsymbol{x}_2), \ldots, u^h(\boldsymbol{x}_N)]^{\mathrm{T}} \\ &= [\Psi^{\mathrm{T}}(\boldsymbol{x}_1)\boldsymbol{a}, \Psi^{\mathrm{T}}(\boldsymbol{x}_2)\boldsymbol{a}, \ldots, \Psi^{\mathrm{T}}(\boldsymbol{x}_N)\boldsymbol{a}]^{\mathrm{T}} \\ &= [\Psi(\boldsymbol{x}_1), \Psi(\boldsymbol{x}_2), \ldots, \Psi(\boldsymbol{x}_N)]^{\mathrm{T}}\boldsymbol{a} = A\boldsymbol{a}\end{aligned} \tag{6}$$

where

$$\begin{aligned}\boldsymbol{A} &= [\Psi(\boldsymbol{x}_1), \Psi(\boldsymbol{x}_2), \ldots, \Psi(\boldsymbol{x}_N)]^{\mathrm{T}} \\ &= \begin{bmatrix} \psi_1(\boldsymbol{x}_1) & \psi_2(\boldsymbol{x}_1) & \cdots & \psi_N(\boldsymbol{x}_1) \\ \psi_1(\boldsymbol{x}_2) & \psi_2(\boldsymbol{x}_2) & \cdots & \psi_N(\boldsymbol{x}_2) \\ \vdots & \vdots & \ddots & \vdots \\ \psi_1(\boldsymbol{x}_N) & \psi_2(\boldsymbol{x}_N) & \cdots & \psi_N(\boldsymbol{x}_N) \end{bmatrix}\end{aligned} \tag{7}$$

Therefore (5) becomes

$$u^h(\boldsymbol{x}) = \Psi^{\mathrm{T}}(\boldsymbol{x})A^{-1}\boldsymbol{u} = \boldsymbol{N}(\boldsymbol{x})\boldsymbol{u} \tag{8}$$

The first-order partial derivative of function $u^h(\boldsymbol{x})$, with respect to the space variables, can be expressed as [18]

$$\frac{\partial u^h(\boldsymbol{x})}{\partial x^i} = \boldsymbol{N}(\boldsymbol{x})_{,i}\boldsymbol{u} \tag{9}$$

where

$$\boldsymbol{N}(\boldsymbol{x})_{,i} = \Psi^{\mathrm{T}}_{,i}A^{-1} = [\psi_{1,i}(\boldsymbol{x}), \psi_{2,i}(\boldsymbol{x}), \ldots, \psi_{N,i}(\boldsymbol{x})]^{\mathrm{T}}A^{-1} \tag{10}$$

and $\psi_{j,i}(\boldsymbol{x}) = \partial\psi_j(\boldsymbol{x})/\partial x^i$.

Formulating a meshless method for solving the DDM equations needs a set of scalar quantity nodes, $\boldsymbol{X}_1 = \{\boldsymbol{x}_{11}, \boldsymbol{x}_{12}, \ldots, \boldsymbol{x}_{1N}\}$, and a set of vector quantity nodes, $\boldsymbol{X}_2 = \{\boldsymbol{x}_{21}, \boldsymbol{x}_{22}, \ldots, \boldsymbol{x}_{2N}\}$, to be distributed over the 2D problem domain. Similar to the conventional FDTD method, $\boldsymbol{X}_1$ and $\boldsymbol{X}_2$ are defined in a way that each $\boldsymbol{X}_1$ node is surrounded by $\boldsymbol{X}_2$ nodes and conversely. Therefore the solution domain is discretised by two sets of scattered nodes, one defining the scalar quantity at the nodal points, $\boldsymbol{X}_1$, and the other defining the vector quantity positioned at the midpoint of the cells of nodal points, $\boldsymbol{X}_2$.

According to (8), the approximation of all components in DDM can be expanded with the same RBF

$$n(\boldsymbol{x}, t) = \boldsymbol{N}(\boldsymbol{x})\upsilon(t) \tag{11}$$

$$\varphi(\boldsymbol{x}, t) = \boldsymbol{N}(\boldsymbol{x})\zeta(t) \tag{12}$$

$$J_x(\boldsymbol{x}, t) = \boldsymbol{M}(\boldsymbol{x})j_x(t), \quad J_y(\boldsymbol{x}, t) = \boldsymbol{M}(\boldsymbol{x})j_y(t) \tag{13}$$

$$E_x(\boldsymbol{x}, t) = \boldsymbol{M}(\boldsymbol{x})e_x(t), \quad E_y(\boldsymbol{x}, t) = \boldsymbol{M}(\boldsymbol{x})e_y(t) \tag{14}$$

where $\upsilon(t)$, $\zeta(t)$, $j_x(t)$, $j_y(t)$, $e_x(t)$ and $e_y(t)$ are unknown time coefficient vectors to be computed at the collocation nodes. The known matrices $\boldsymbol{N}$ and $\boldsymbol{M}$ are determined by forcing the interpolation (6) to pass through $\boldsymbol{X}_1$ and $\boldsymbol{X}_2$, respectively. Thus, (1)–(3) are discretised using (11)–(14)

doi: 10.1049/iet-map.2010.0281

and finite-difference approximation of the time derivative, as

$$\boldsymbol{N}\upsilon^{k+1} = \boldsymbol{N}\upsilon^{k} + (\boldsymbol{M}_{,x}j_x^k + \boldsymbol{M}_{,y}j_y^k)/q \tag{15}$$

$$[\boldsymbol{N}_{,xx} + \boldsymbol{N}_{,yy}]\zeta^{k+1} = -q(N_{\mathrm{d}} - \boldsymbol{N}\upsilon^{k+1})/\varepsilon \tag{16}$$

$$\boldsymbol{M}j_i^{k+1} = -qn\mu_n\boldsymbol{N}_{,i}\zeta^{k+1} + qD_n\boldsymbol{N}_{,i}\upsilon^{k+1}; \quad i = x, y \tag{17}$$

$$\boldsymbol{M}e_i^{k+1} = -\boldsymbol{N}_{,i}\zeta^{k+1}; \quad i = x, y \tag{18}$$

The calculations of unknowns are simple and straightforward from (15)–(18). Besides, $\boldsymbol{N}^{-1}$ and $\boldsymbol{M}^{-1}$ must be calculated only once for the constant collocation points throughout the computations. Therefore computing υ^{k+1}, ζ^{k+1}, j^{k+1} and e^{k+1} becomes simple operations of $O(\boldsymbol{N})$.

Similarly, as in finite-difference methods, (15) is conditionally stable. However, the stability of the scheme can be easily preserved by automatic and progressively discarded time subdivisions as suggested in [19]. The time-step size Δt in the explicit methods for the semiconductor equations is a function of the average carrier velocity v_{d} and the spatial steps Δx and Δy to comply with the following CFL condition for stability and minimising the numerical dispersion [14]

$$v_{\mathrm{d}}\Delta t \le [\Delta x^{-2} + \Delta y^{-2}]^{-1/2} \tag{19}$$

To drive the implicit scheme, the θ-weighting approach is used for the time derivative in the combination of (1) and (2). Therefore (15) is changed to

$$\begin{aligned}&\{\boldsymbol{N} - \Delta t\theta\cdot[\mu_n\nabla\cdot E^{k+1}\boldsymbol{N} + \mu_n E^{k+1}\cdot\nabla\boldsymbol{N} + D_n(\boldsymbol{N}_{,xx} + \boldsymbol{N}_{,yy})]\}\upsilon^{k+1}\\ &\quad = \{\boldsymbol{N} + \Delta t(1-\theta)\cdot[\mu_n\nabla\cdot E^{k}\boldsymbol{N}\\ &\qquad + \mu_n E^{k}\cdot\nabla\boldsymbol{N} + D_n(\boldsymbol{N}_{,xx} + \boldsymbol{N}_{,yy})]\}\upsilon^{k}\end{aligned} \tag{20}$$

where $0 \le \theta \le 1$. It must be noted that (20) is written in a manner so as to be independent of j^{k+1} and moreover by using (14) and (18), E^{k+1} can be placed with ζ^{k+1}. Therefore (20) has only scalar parameters, that is, υ and ζ for n and φ, respectively. Besides a reduction of calculation time because of reduced matrix dimensions, the application of boundary conditions is simpler in this kind of presentation.

We will use $\theta = 1/2$, that is, Crank–Nicholson scheme. The first-order upwind scheme

$$v_i\frac{d}{\mathrm{d}x}[f_i] = \begin{cases} v_i(f_i - f_{i-1})/\Delta x & \text{if } v_i \ge 0 \\ v_i(f_{i+1} - f_i)/\Delta x & \text{if } v_i < 0 \end{cases} \tag{21}$$

is used for spatial derivatives of the advection terms of (20), which means only the upstream points are brought up in calculations. For example, we have

$$E\cdot\nabla\boldsymbol{N} = 0.5\left(\left|E_x\frac{\partial r_{ij}}{\partial x}\right| + E_x\frac{\partial r_{ij}}{\partial x} + \left|E_y\frac{\partial r_{ij}}{\partial y}\right| + E_y\frac{\partial r_{ij}}{\partial y}\right)\boldsymbol{N}_{,r} \tag{22}$$

in our 2D problem, where $r_{ij} = [(x_i - x_j)^2 + (y_i - y_j)^2]^{1/2}$. If in (20), E^{k+1} is approximated by E^k (semi-implicit approximation), computing unknowns becomes simple and straightforward using (16) and (20). Similar to the explicit meshfree method, computation of υ^{k+1} and ζ^{k+1} are simple $O(\underline{\boldsymbol{N}})$ operations if the collocation points do not change during the simulation. The proof of the stability of such a system is simple but a numerical approach is required to find the eigenvalues of the coefficient matrix [20]. Instead, we tested the method by increasing the time step. If $\{\Delta t_{\mathrm{FDTD}}\}_{\mathrm{DDM}}$ is the maximum value of time-step size from (19), the results for an example large time-step size $\Delta t = 200\{\Delta t_{\mathrm{FDTD}}\}_{\mathrm{DDM}}$ show the stability of the method while $\theta = 1/2$. As discussed in Section 6, we use $\Delta t = 100\{\Delta t_{\mathrm{FDTD}}\}_{\mathrm{DDM}}$ in the DC and $\Delta t = 10\{\Delta t_{\mathrm{FDTD}}\}_{\mathrm{DDM}}$ in the full-wave simulations.

4 Electromagnetic model

Maxwell's equations characterise electromagnetic wave propagation completely, which can be written in a matrix form [21] as

$$\partial_t W = (D_1 + D_2)W + J \tag{23}$$

where

$$W = [E_x \quad E_y \quad E_z \quad H_x \quad H_y \quad H_z]$$

$$J = [J_x \quad J_y \quad J_z \quad 0 \quad 0 \quad 0]$$

$$D_1 = \begin{bmatrix} 0 & 0 & 0 & 0 & -a_1\partial_z & 0 \\ 0 & 0 & 0 & 0 & 0 & -a_1\partial_x \\ 0 & 0 & 0 & -a_1\partial_y & 0 & 0 \\ 0 & 0 & -a_2\partial_y & 0 & 0 & 0 \\ -a_2\partial_z & 0 & 0 & 0 & 0 & 0 \\ 0 & -a_2\partial_x & 0 & 0 & 0 & 0 \end{bmatrix}$$

$$D_2 = \begin{bmatrix} 0 & 0 & 0 & 0 & 0 & a_1\partial_y \\ 0 & 0 & 0 & a_1\partial_z & 0 & 0 \\ 0 & 0 & 0 & 0 & a_1\partial_x & 0 \\ 0 & a_2\partial_z & 0 & 0 & 0 & 0 \\ 0 & 0 & a_2\partial_y & 0 & 0 & 0 \\ a_2\partial_y & 0 & 0 & 0 & 0 & 0 \end{bmatrix}$$

$$a_1 = \frac{1}{2\varepsilon}, \quad a_2 = \frac{1}{2\mu}$$

In the above equations, E is the electric field, H is the magnetic field, J is the total current density, ε and μ are the electric permittivity and the magnetic permeability, respectively. To solve (23), the algorithm of ADI-FDTD introduced by Namiki [12] and Zheng *et al.* [13] is used to eliminate the constraints of the CFL condition

$$v_{P\,\max}\Delta t \le [\Delta x^{-2} + \Delta y^{-2} + \Delta z^{-2}]^{-1/2} \tag{24}$$

in the standard FDTD. In the above equation $v_{P\max}$ is the maximum of wave phase velocity within the model. In the ADI scheme, (23) is broken up into two time steps at $n + 1/2$ and $n + 1$ as

$$(I - D_1)W^{n+1/2} = (I + D_2)W^n + 0.5J^n \tag{25}$$

$$(I - D_2)W^{n+1} = (I + D_1)W^{n+1/2} + 0.5J^{n+1/2} \tag{26}$$

where J is the estimated current density by (12).

5 Computational procedure

Several choices are possible as RBF $\psi(\boldsymbol{x}, \boldsymbol{x}_i)$, for example, multi-quadratics (MQ) or spline functions. In this paper, the following compactly supported RBF proposed by Wu [10] is used

$$\psi(\boldsymbol{x}, \boldsymbol{x}_i) = \psi(r_i) = \begin{cases} (1-r_i)^4(4+16r_i+12r_i^2+3r_i^3), & r_i \le 1 \\ 0, & \text{elsewhere} \end{cases} \quad (27)$$

where $r_i = \|\boldsymbol{x} - \boldsymbol{x}_i\|/d_{mi}$. Here, d_{mi} represents the supported domain radius at the collocation node $\boldsymbol{x}_i$ as

$$d_{mi} = d_{\max} C_i \quad (28)$$

where $d_{\max}$ is a scaling parameter and C_i at a particular node is determined by searching for enough neighbour nodes such that $\boldsymbol{A}$ is non-singular everywhere in the domain. Selecting the RBF type is based on the fact that it has good accuracy without the extra load of computing the shape parameters which are needed in other accurate approximations such as MQ [22]. On the other hand, the use of a compactly supported version of the RBF kernel could result in a sparse matrix, and thus the computational cost and memory requirements are reduced [11].

The coupling between the two models is found out by properly transforming the physical parameters (e.g. fields and current densities) from one model to the other. In each time-step, Maxwell's and semiconductor equations should be solved sequentially. First, Maxwell's equations are solved for the electric and magnetic field distributions using the current density existed from previous time step. Then, the earned electromagnetic (EM) fields are used in the semiconductor equations to find the new current density. This process is repeated for each time interval [1, 14]. The full-wave analysis procedure includes the following parts.

5.1 Steady-state DC solution (Initialisation)

The steady-state DC solution for electric fields, current densities and the other transport parameters are obtained from the semiconductor model by solving Poisson's and the hydrodynamic transport equations. The device is biased and the DC parameter distributions E, n, φ and J_{DC} are obtained by solving (14)–(17) in the explicit and (15)–(18) in the implicit case. This DC solution serves as the corresponding initial values inside the active device model.

5.2 Time-domain AC solution

After completing the initialisations, the AC excitation is applied, that is, $J = J_{\mathrm{DC}} + J_{\mathrm{AC}}$. The time-domain distribution of the EM fields is obtained using Maxwell's equations. These EM fields are used by the semiconductor model to update the current density. More details about AC and DC solutions can be found in [1]. Fig. 1 shows flowchart of the sequence of the complete scheme for full-wave simulation of a semiconductor device containing active device model and electromagnetic models, simulated using meshfree and ADI-FDTD methods, respectively.

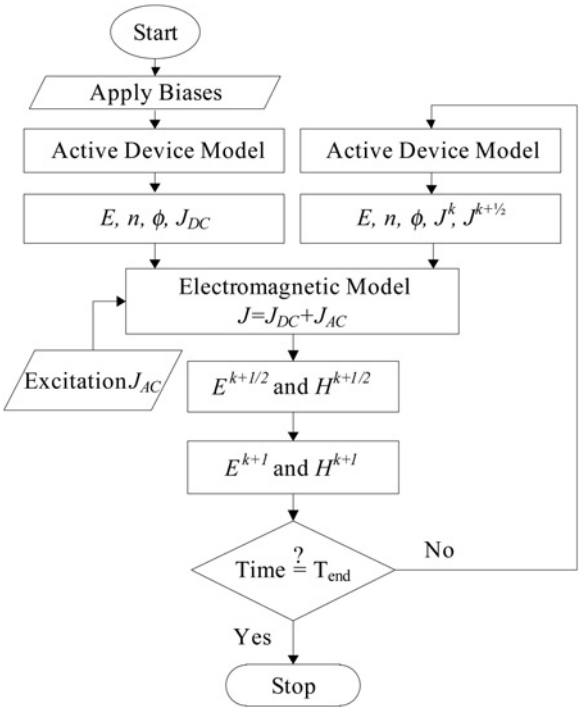

Fig. 1 *Flowchart of the sequence of full-wave simulation of a semiconductor device*

6 Simulation results

To demonstrate the performance of the proposed approach, the GaAs MESFET transistor shown in Fig. 2 is considered. This transistor has an electromagnetic source excitation with $f_{\max} = 100$ GHz, large applied electric field, and heavily doped $N_{\mathrm{d}} = 2 \times 10^{17}$ cm^{-3}.

As the system of equations for active device model and electromagnetic model must be solved simultaneously, the cell size is chosen equal to 0.01 μm for the x- and y- directions [1] and 1 μm for the z-direction. Since the nodes are uniformly spaced in this example, the values of C_i and $d_{\max}$ in (28) are set to the distance between two adjacent nodes and 1, respectively. From (19), (24) and the above cell sizes, the time-step size for the explicit FDTD method must be chosen to be less than 0.01 fs. Actually (24) determines the time-step limit for this method. If we use an explicit meshfree method for the active device model and the ADI-FDTD method for the electromagnetic model (half-implicit scheme), limitation (24) is removed and the time-step size can be chosen up to 1 fs that is determined by (19).

Using the maximum allowable time-step size 1 fs, for the half-implicit scheme, the number of simulation time steps is reduced by a factor 100 with respect to the explicit scheme. However, the simulation time of one time step in our ADI-FDTD program is equal to the simulation time of five time steps in the FDTD program. Hence the half-implicit simulation will be performed 20 times faster than the conventional FDTD simulation. The larger time-step size increases the numerical dispersion error

$$p = 1 - v_{\mathrm{p}}/c \quad (29)$$

doi: 10.1049/iet-map.2010.0281

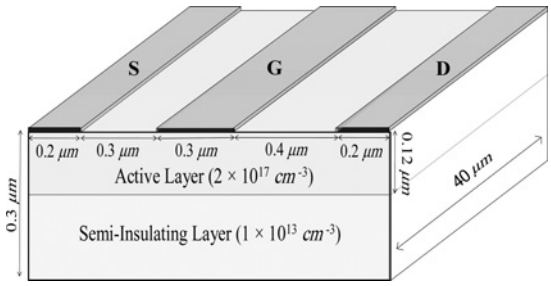

Fig. 2 *Simulated MESFET structure*

from 5×10^{-7}% for the FDTD method to 10^{-4}% for the ADI-FDTD method. In (29), v_p is the phase velocity of the numerical wave and c is the theoretical velocity of the wave.

The simulation time can be further reduced using the implicit meshfree and the implicit ADI-FDTD methods for solving active device and electromagnetic equations, respectively (full-implicit scheme). Using the implicit methods removes the time-step size limits in (19) and (24) and the time-step size can be selected as more than 1 fs. Although the full-implicit method is unconditionally stable, the time-step size is determined by a simple approach [23] to achieve the desired numerical dispersion accuracy. The numerical dispersion error, p, is given by

$$\sin\left(\frac{\pi}{(1-p)N}\right) = \frac{\tan(\pi s/N)}{s} \tag{30}$$

where $s = c\ \Delta t/\Delta_{\max}$ is the Courant number, $N = \lambda/\Delta_{\max}$ is the minimum mesh density corresponding to the maximum mesh size $\Delta_{\max}$, and c is the theoretical velocity.

In the full-wave simulation, the cell size is imposed by the Debye length, which is much smaller than the practical wavelengths [14]. Thus, the Courant-Friedrich-Levy number ((CFLN) = $(\Delta t_{\mathrm{ADI-FDTD}})/(\Delta t_{\mathrm{FDTD}})$) can be large and still the numerical dispersion error of the method remains small. As (30) is a non-linear equation with respect to Δt, we select a proper Δt to have enough samples from input and output signals and some harmonics of them in the simulated time. Then if the calculated p from (30) by this Δt is not satisfactory, a smaller Δt is tested until the value of p is acceptable. In our example, $f_{\max}$ and $\Delta_{\max}$ are equal to 100 GHz and 1 μm, respectively. By selecting $\Delta t = 10$ fs the numerical dispersion accuracy is obtained equal to an acceptable value of 0.03% and we have 1000 samples in each period of output signals, which is enough to show non-linear effects. If we need to reduce the numerical dispersion error from the above value, higher-order ADI-FDTD methods are applicable.

6.1 DC simulation

The device is biased to $V_{ds} = 2$ V and $V_{gs} = -0.5$ V. The state of the MESFET under DC steady state is represented by the distribution of potential and carrier density. It is to be noted that Dirichlet boundary conditions are used at the electrodes while Neumann's boundary conditions are used at the other walls. As the DC simulation is not to contain the electromagnetic model, a larger time-step $\Delta t = 0.1$ *ps* is selected for this part. Fig. 3 shows the DC potential and carrier density distributions obtained using the implicit meshfree method. A comparison between results of explicit FDTD, explicit meshfree and semi-implicit meshfree methods are provided in Figs. 4 and 5. It is significant to indicate that

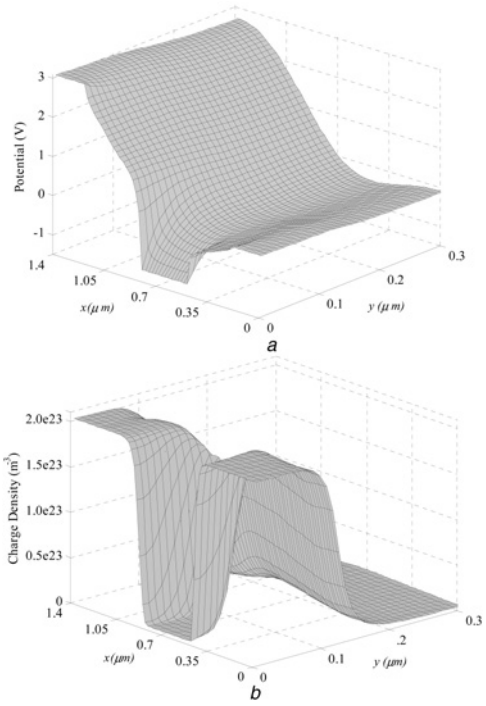

Fig. 3 *DC simulation results by the proposed algorithm*

a Potential distribution
b Carrier density distribution

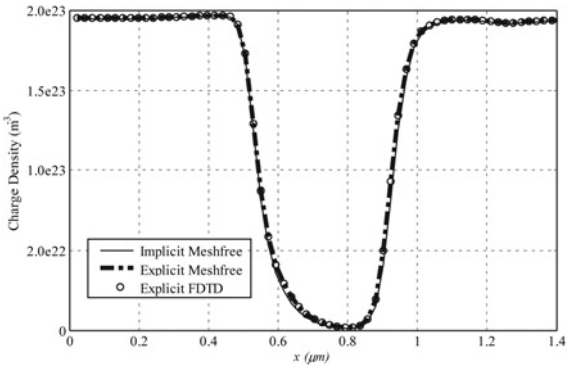

Fig. 4 *Charge density across the 'x'-direction at 'y = 0.09 μm' for different methods*

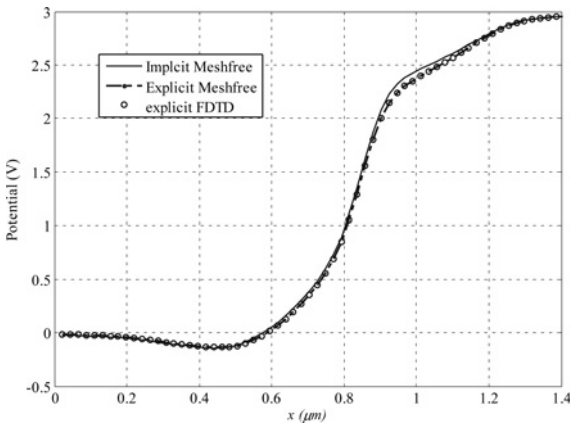

Fig. 5 *Potential distribution across the 'x'-direction at 'y = 0.09 μm' for different methods*

different methods give precisely the same results. For a specific discretisation, the simulation times for explicit FDTD and explicit meshfree methods are nearly equal whereas the implicit meshfree method will be twice as fast as explicit methods. Since in a full-wave semiconductor simulation the required CPU time for 2D active device simulation is much smaller than the required CPU time of 3D electromagnetic simulation in each simulation time step, we do not need a very fast method for active device simulation. In fact, the aim of the implicit method for active part is reduction of the total number of simulation time steps when simulating active and electromagnetic models simultaneously.

After calculating the distributions of potential and carrier density from the DC solution, we can find out where quantities vary rapidly and slowly. Then in domains where the variation of parameters is low, the node generator subprogram removes some nodes from the early uniform node distribution. With this method, we can create a non-uniform node distribution that is dense only where required. The non-uniform node distribution produced by the DC solution can be used in the AC analysis because the DC solution is the initial value of AC analysis and the level of AC excitation is lower than the DC level at most times. Using a proper non-uniform node distribution can reduce the total simulation time.

6.2 AC simulation

In the AC simulation we have electromagnetic wave propagation, therefore absorbing boundary conditions are considered in the electromagnetic simulation part. We have used the unconditionally stable ADI-CPML method [24] for boundary conditions because of desirable reflection properties even for large values of CFLN. The boundary conditions for the active device part of the simulation are the same as the boundary conditions in the DC simulation. An AC excitation is applied to the gate electrode, which is given as $V_{gs}(t) = V_{gs0} + \Delta v_{gs} \sin(\omega t)$, where V_{gs0} is the DC bias applied to the gate electrode, ω is the angular frequency of the applied signal and Δv_{gs} is the peak value of the AC signal (0.1 V). Fig. 6 shows the output drain voltage obtained by multiplying the total current by the resistance that defines the DC operating point of the transistor [25]. As can be seen, the results in the explicit (conventional FDTD for both models), the half-implicit (ADI-FDTD for electromagnetic model and explicit meshfree for active device model) and the full-implicit (ADI-FDTD for electromagnetic model and semi-implicit meshfree for active device model) cases are in good agreement. As expressed before, the time for calculating one time step of the active device model is much less than the similar time for the electromagnetic model. Thus, there is no significant difference between calculation time of one time step in the half-implicit and full-implicit schemes. Therefore as the number of simulation time steps in the full-implicit case is reduced by a factor 10 with respect to the half-implicit case, the simulation will be approximately ten times faster. In comparison with the conventional FDTD method, when Δt increases from 0.01 to 10 fs, the full-implicit method is 200 times faster while the numerical dispersion error is still small. The total numbers of simulation time steps are 2×10^6, 2×10^4 and 2×10^3 with the estimated simulation times of 24 days, 2 days and 4 h for the explicit, the half-implicit and the full-implicit methods, respectively. A PC with a Pentium 4 processor (2.5 GHz) and 2 GB RAM was used in these simulations.

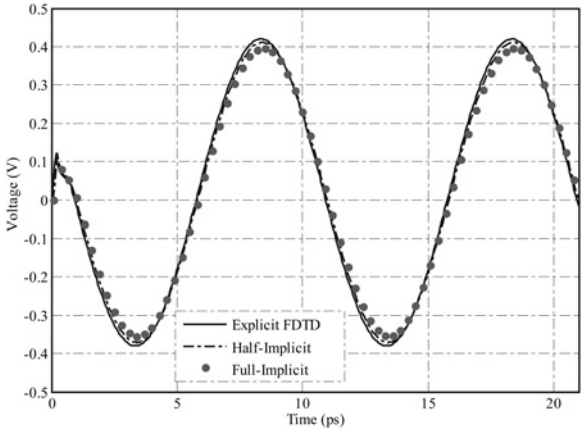

Fig. 6 *Output drain voltage from explicit FDTD ($\Delta t = 0.01$ fs), half-implicit ($\Delta t = 1$ fs) and full-implicit ($\Delta t = 10$ fs) methods*

7 Conclusion

We have proposed a numerical method for simulation of the time-dependent drift-diffusion model of semiconductor devices in two dimensions. The method is simple, especially for complicated domains and higher dimensions. Between RBFs a compactly supported version has been chosen since it can result in a sparse matrix, and thus decrease the computational cost and memory requirements. Possible extensions of this research are to consider adaptive data nodes and overlapping domain decomposition method to reduce the CPU time.

We have also proposed a numerical method for full-wave simulation of the time-dependent semiconductor device equations with a much lower calculation time in comparison with conventional methods. In the full-implicit scheme, we simulate the electromagnetic and active device equations simultaneously with the ADI-FDTD and semi-implicit meshfree approaches, respectively. This scheme is a full-implicit method and allows increasing of the time step until the numerical dispersion accuracy is still acceptable. Since the size of the local minimum cell in the computational domain (which is imposed by the Debye length) is much smaller than the wavelength, the error limit is larger than the CFL limit. Therefore the full-implicit method is more efficient than the conventional explicit FDTD method for the full-wave simulation of active micro/mm-wave devices. In an example, we achieve a 99% reduction in the simulation time by using this approach while still having a good degree of accuracy in comparison with the explicit method.

8 Acknowledgment

The authors would like to express their appreciation to Professor W.H.A. Schilders, Centre for Analysis, Scientific computing, and Applications (CASA), Eindhoven University of Technology (TU/e), Eindhoven, The Netherlands, for his help and guidance. This work was supported in part by the Education & Research Institute for ICT.

9 References

1 Alsunaidi, M.A., Imtiaz, S.M.S., El-Ghazaly, S.M.: 'Electromagnetic wave effects on microwave transistors using a full-wave time-domain model', *IEEE Trans. Microw. Theory Tech.*, 1996, **44**, pp. 799–808

2 Imtiaz, S.M.S., El-Ghazaly, S.M.: 'Global modeling of millimeter-wave circuits: electromagnetic simulation of amplifiers', *IEEE Trans. Microw. Theory Tech.*, 1997, **45**, pp. 2208–2216

3 Feng, Y.K., Hintz, A.: 'Simulation of sub-micrometer GaAs MESFET's using a full dynamic transport model', *IEEE Trans. Electron Devices*, 1988, **35**, pp. 1419–1431

4 Liu, Q.H., Cheng, C., Massoud, H.Z.: 'The spectral grid method: a novel fast Schrödinger-equation solver for semiconductor nanodevice simulation', *IEEE Trans. Comput. Aided Des. Integr. Circuit Syst.*, 2004, **23**, pp. 1200–1208

5 Cheng, C., Lee, J.-H., Lim, K.H., Massoud, H.Z., Liu, Q.H.: '3D quantum transport solver based on the perfectly matched layer and spectral element methods for the simulation of semiconductor nanodevices', *J. Comput. Phys.*, 2007, **227**, pp. 455–471

6 Belytschko, T., Krongauz, Y., Organ, D., Fleming, M., Krysl, P.: 'Meshless methods: an overview and recent developments', *Comput. Methods Appl. Mech. Eng.*, 1996, **139**, pp. 3–47

7 Kansa, E.J.: 'Multiquadrics – a scattered data approximation scheme with applications to computational fluiddynamics. II. Solutions to parabolic, hyperbolic and elliptic partial differential equations', *Comput. Math. Appl.*, 1990, **19**, pp. 147–161

8 Zerroukat, M., Power, H., Chen, C.S.: 'A numerical method for heat transfer problems using collocation and radial basis functions', *Int. J. Numer. Methods Eng.*, 1998, **42**, pp. 1263–1278

9 Li, J., Cheng, A.H.-D., Chen, C.S.: 'A comparison of efficiency and error convergence of multiquadric collocation method and finite element method', *Eng. Anal. Bound. Elem.*, 2003, **27**, pp. 251–257

10 Wu, Z.M.: 'Compactly supported positive definite radial functions', *Adv. Comput. Math.*, 1995, **4**, pp. 283–292

11 Carlson, R., Foley, T.: 'The parameter R2 in multiquadric interpolation', *Comput. Math. Appl.*, 1991, **21**, pp. 29–42

12 Namiki, T.: '3-D ADI-FDTD method – unconditionally stable time-domain algorithm for solving full vector Maxwell's equations', *IEEE Trans. Microw. Theory Tech.*, 2000, **48**, pp. 1743–1748

13 Zheng, F., Chen, Z., Zhang, J.: 'Toward the development of a three-dimensional unconditionally stable finite-difference time-domain method', *IEEE Trans. Microw. Theory Tech.*, 2000, **48**, pp. 1550–1558

14 Movahhedi, M., Abdipour, A.: 'Efficient numerical methods for simulation of high-frequency active devices', *IEEE Trans. Microw. Theory Tech.*, 2006, **54**, pp. 2636–2645

15 Mirzavand, R., Abdipour, A., Moradi, G., Movahhedi, M.: 'Full-wave semicoductor devices simulation using ADI-FDTD method', *Prog. Electromagn. Res. M*, 2010, **11**, pp. 191–202

16 Grasser, T., Tang, T.W., Kosina, H., Selberherr, S.: 'A review of hydrodynamic and energy-transport models for semiconductor device simulation', *Proc. IEEE*, 2003, **91**, pp. 251–274

17 Zhou, X., Tan, H.S.: 'Monte Carlo formulation of field-dependent mobility for AIxGa1-xAs', *Solid-Sate Electro.*, 1995, **38**, pp. 1264–1266

18 Lai, S.J., Wang, B.Z., Duan, Y.: 'Application of the RBF-based meshless method to solve 2-D time domain Maxwell's equations'. Int. Conf. on Microwave and Millimeter Wave Technology, Nanjing, China, 2008

19 Zerroukat, M., Chatwin, C.R.: 'A more accurate FD solution for the 3D non-linear heat equation', *Commun. Numer. Meth. Eng.*, 1995, **11**, pp. 535–544

20 Zerroukat, M., Djidjeli, K., Charafi, A.: 'Explicit and implicit meshless methods for linear advection-diffusion-type partial differential equations', *Int. J. Numer. Meth. Eng.*, 2000, **48**, pp. 19–35

21 Guilin, S., Trueman, C.W.: 'Efficient implementations of the Crank–Nicolson scheme for the finite-difference time-domain method', *IEEE Trans. Microw. Theory Tech.*, 2006, **54**, pp. 2275–2284

22 Hamers, B., Suykens, J.A.K., Moor, B.D.: 'Compactly supported RBF kernels for sparsifying the gram matrix in LS-SVM regression models', Artificial Neural Networks-ICANN, Spain

23 Carlson, R., Foley, T.: 'The parameter R^2 in multiquadric interpolation', *Comput. Math. Appl.*, 1991, **21**, pp. 29–42

24 Gedney, S.D., Liu, G., Roden, J.A., Zhu, A.: 'Perfectly matched layer media with CFS for an unconditionally stable ADI-FDTD method', *IEEE Trans. Antennas Propag.*, 2001, **49**, pp. 1554–1559

25 Hussein, Y.A., El-Ghazaly, S.M.: 'Extending multiresolution timedomain (MRTD) technique to the simulation of high-frequency active devices', *IEEE Trans. Microw. Theory Tech.*, 2003, **51**, pp. 1842–1851